Ageing simulation of a hydraulic engine mount: A data-informed finite element approach

Soltani, P, Pinna, C, Wagg, DJ & Whear, R

Ageing Simulation of a Hydraulic Engine Mount – a Data Informed Finite Element Approach

Corresponding author: Payam Soltani

ᵃ Faculty of Engineering, Environment & Computing, Coventry University, Coventry, CV12JH, UK

Emails : payam.soltani@coventry.ac.uk , payam.soltani@gmail.com

Christophe Pinnaᵇ,
ᵇ Department of Mechanical Engineering, The University of Sheffield, S13JD, UK
Email: c.pinna@sheffield.ac.uk

David .J. Waggᵇ,
ᵇ Department of Mechanical Engineering, University of Sheffield, S13JD, UK
Email: david.wagg@sheffield.ac.uk

Roly Whearᶜ,
ᶜJaguar Land Rover Ltd, CV35 0RR, UK
Email: rwhear1@jaguarlandrover.com

Acknowledgment

Ageing Simulation of a Hydraulic Engine Mount – a Data Informed Finite Element Approach

P. Soltani[a] *, C. Pinna[b], D.J. Wagg[b], and R.Whear[c],

[a] Faculty of Engineering, Environment & Computing, Coventry University, Coventry, CV12JH, UK

[b] Department of Mechanical Engineering, The University of Sheffield, S13JD, UK

[c]Jaguar Land Rover Ltd, CV35 0RR, UK

Abstract

Hydraulic engine mounts (EMs) are key elements in an automotive vehicle suspension system that typically experience a change of their designed function during their working lifetime due to progressive material ageing, primarily from the elastomeric component. Ageing of the EM, resulting from severe and continuous mechanical and thermal loads, can have a detrimental impact on the ride and comfort and long-term customer satisfaction. This paper introduces a new practical methodology for simulating the ageing behaviour of EMs resulting from the change in properties of their elastomeric main spring (MS) component. To achieve this, a set of dynamic mechanical thermal analysis (DMTA) tests were conducted on elastomeric coupons taken from a set of EMs with different service and ageing conditions. These experimental results were used to characterise the change in mechanical response of the elastomer and to build up an empirical elastomer ageing model (EAM). Then a finite element (FE) model of the MS was developed that used the EAM, so that the ageing behaviour of the EM could be simulated. The resulting ageing model was verified by using experimental results from a second batch of ex-service EMs. The results show an increasing trend of the vertical static stiffness of the EMs with distance travelled (or age) up to a certain distance (approximately 95000 km). The trend is then reversed and a softening effect is observed. Moreover, the results reveal that both the maximum stiffness value and the distance travelled at the peak stiffness decrease as the temperature increases.

Keywords: Hydraulic engine mount, Elastomer, Ageing, Material degradation, Finite element, Simulation

---

*Corresponding author, Email: payam.soltani@coventry.ac.uk , payam.soltani@gmail.com

1. Introduction

The drive to improve long-term customer satisfaction and to extend vehicle warranties (with associated claim costs), along with modern trends for optimisation of engineering design and decision making through virtual prototyping, has created a need in the automotive industry for the development of ageing simulations. One particular example, at component level, is concerned with the change in the mechanical response of engine mounts (EMs) over time due to, among other effects, the evolution of the mechanical properties of the constitutive elastomer. Understanding the material and mechanical performance of elastomers and elastomeric components over their designed and planned service life has been an active research topic for nearly two decades [1-4].

Hydraulic EMs are typically used as passive vibration absorbers, which suppress and isolate the noise and vibration created by the engine and are considered to be key elements in the suspension system to control the noise, vibration, and harshness (NVH) level in vehicles [5]. As the time in service of the EM increases, its mechanical and dynamical response deviate from the original design and the noise and vibration levels increase [6]. This will affect the ride comfort and vehicle performance and consequently, customer satisfaction as the vehicle ages.

The change in EM characteristics is typically attributed to the change in material properties (especially stiffness) of the elastomeric component inside the mount, termed the main spring (MS) [7]. The MS provides the static stiffness and flexibility of the EM, and its ageing does clearly affect its response and attenuating efficiency [8]. Understanding the effect of stiffness change of the MS on the ageing behaviour of the EMs is therefore crucial for engineers and designers concerned with improving and optimising the design of the suspension system. This can also help

the automotive industry reduce maintenance costs and improve customers' satisfaction.

Few studies on the modelling and simulation of the ageing behaviour of EMs are available in the literature. Although some studies investigated the ageing effects on the mechanical behaviour of the elastomers, most were focused on the material ageing under laboratory conditions [6, 7, 9-11]. However, the variability of the mechanical/thermal loading and environmental conditions on the EMs during their service life and also the complexity of the ageing phenomenon for elastomers are highly challenging to recreate under laboratory conditions.

The main aim of this paper is to introduce a practical methodology for the ageing simulation of EMs used in service as material ageing occurs in the elastomeric MS. This will be done using a data informed finite element (FE)-based modelling technique, using empirical data derived from experimental measurements of changes in material properties of the elastomers aged under real and operational conditions.

This paper is divided into the following sections. In Section 2 the functioning of the EM under investigation is explained. The deviation of the mechanical behaviour of the EM from its original design, due to ageing of the elastomeric MS with time, is also described. Possible ageing mechanisms for elastomers are also introduced in this Section. The details of the dynamic mechanical thermal analysis (DMTA) carried out on the elastomeric coupons of the ex-service EMs (EMs with different service lives and real ageing conditions) are described in Section 3 and the corresponding results are explained. The FE modelling approach of the elastomeric MS of the EM along with its experimental verification procedure is given in Section 4. The simulated ageing behaviour of the EMs is presented in Section 5 with validation from a new batch of ex-service EMs. Conclusions are drawn in Section 6.

4

2. Hydraulic Engine Mount and Ageing Modelling Procedure

The EM under investigation is shown in Figure 1-a and the internal parts and components are depicted in Figure 1-b. The main task of the EM is to reduce and isolate noise and vibration generated by the engine from being transmitted to the chassis and also to support the engine weight. The damping characteristics of the EM are controlled through a fluid moving between the working chamber (or the upper chamber) and the compensation chamber (or the lower chamber) shown in Figure 1-b.

The MS is the only flexible component inside the EM. It consists of an elastomeric spring bolted to the engine from its top surface, and it deforms with relative vibrations between the engine and the chassis.

(a)   (b)
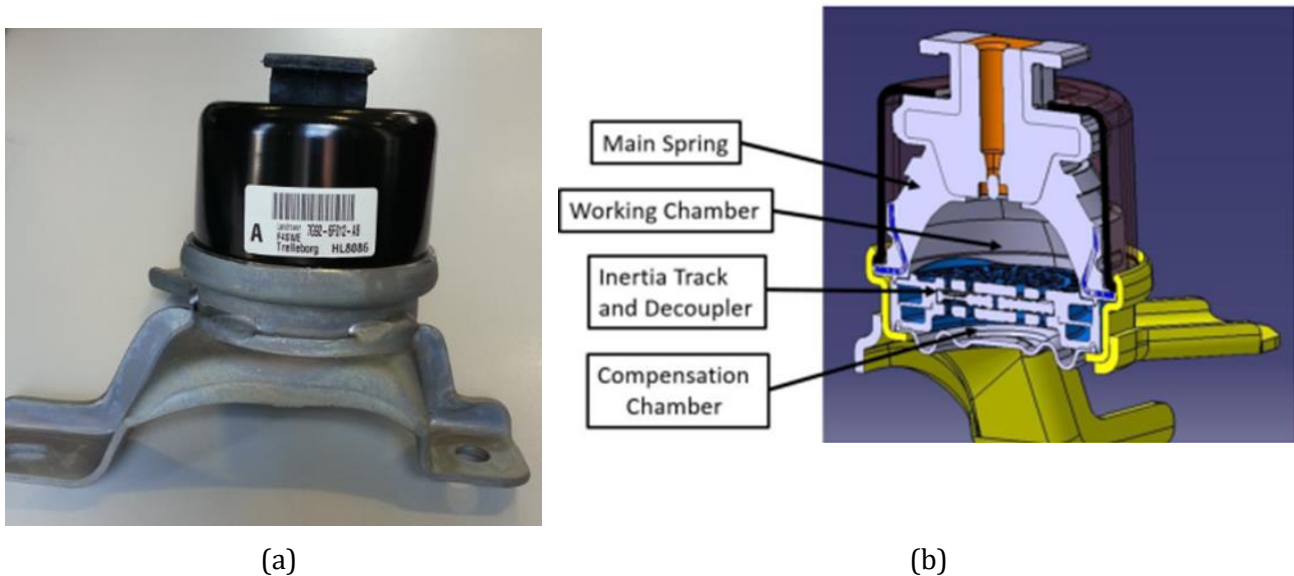
Figure 1 (a) Hydraulic EM (b) cross section of the EM, showing the components of the Hydraulic EM.

The MS (shown in Figure 2) contains three different material components. The main elastomer component (elastomer spring) which acts as the main elastic component and gives the EM its flexibility and the ability to support the engine loads. The elastomer under analysis is a carbon black filled, sulphur-cured natural rubber that forms the MS. The formulation and the accurate proportion of carbon

black filler and other additives within the rubber are unknown. Also shown is the aluminium rib that is embedded within the elastomer and which provides rigidity to the MS, and third part is the aluminium tip that provides a means to connect the engine to the EM. The main task of this part is to transfer the dynamic movements and corresponding kinetic energy, created by the engine body, into the fluid in the compensation chamber and also into the structure of the EM. Moreover, the MS provides static stiffness (K_{St}) to the EM. Dynamic stiffness of the EM will be function of the static stiffness and also the dynamic motion of the fluid inside the chambers of the EM [8].

Throughout the service life, the MS experiences a range of variable mechanical/thermal loadings and environmental conditions and, as a result, the mechanical performance of the MS deviates due to material changes of its elastomer. Elastomer ageing is significantly affected by the operational and environmental conditions of use [13]. Temperature, moisture, UV light, ozone/chemical attack, applied load types and load conditions are all important factors, which affect the degradation of elastomers [11]. Given the nature of the MS that forms the basis of this study and its operational environment and function, the most significant and relevant factors are temperature, fluid absorption and mechanical loading.
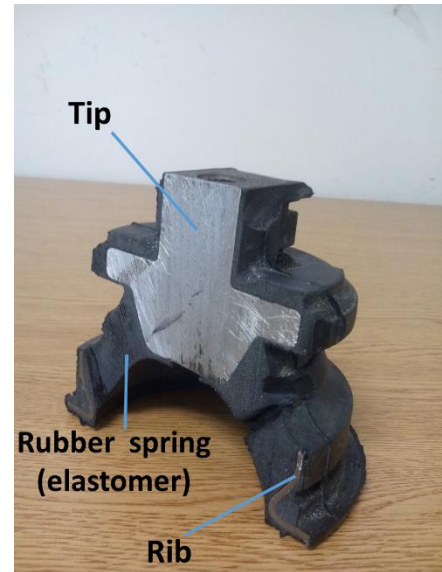
| (a) | (b) |

Figure 2 (a) The main spring (MS) of the EM and (b) its cross-section.

The primary mechanism of ageing for the elastomers in the MS is as yet unknown. However, the ageing mechanisms of elastomers can be categorized into a few types of microstructure alterations:

- Change in the crosslink density of the elastomer caused by post-curing [14] and/or thermal degradation [15, 16].
- Chain-scission caused by oxidative and/or thermal degradations [17].
- Physical changes in microstructures of the elastomers due to particle migration (carbon migration), and crack propagations[15, 16, 18, 19].

Material ageing phenomena in the MS of the EM are inherently complicated especially when the elastomeric components are exposed to long-term complex mechanical, thermal and environmental conditions. Hence, it is very hard to specify the individual contribution of each ageing factor, along with their underlying related ageing mechanisms, on the overall material deterioration of the elastomer. These ageing mechanisms have a direct impact on the mechanical characteristics of the elastomer, especially on its modulus. This, in turn, can

directly influence the mechanical response of the EM through a variation of the static stiffness K_{St} . The static stiffness K_{St} can be measured simply through a vertical force - displacement test on the complete EM and is a key parameter to characterise its static performance. Any change in elastomer properties due to ageing therefore has a direct effect on the static stiffness K_{St}. It should be noted that the dynamic stiffness of the EM (K_{Dyn}) is also function of K_{St} and dynamic motion of the fluid inside the EM. Hence, any change in K_{St} will lead to change in dynamic behaviour of the EM as well.

The first step in the simulation of the ageing behaviour of the EM, in terms of the variation of static stiffness K_{St}, is to create an elastomer ageing model (EAM). This ageing model is aimed at predicting the variation of material properties of the elastomer for different ageing conditions. To construct the model, experimental measurements conducted on elastomer coupons cut from both new and old EMs collected from vehicles after different distance travelled and real ageing conditions are used. The EAM can then be coupled to the FE model of the MS in order to simulate the ageing behaviour of the EM. The simulation procedure is shown in Figure 3.

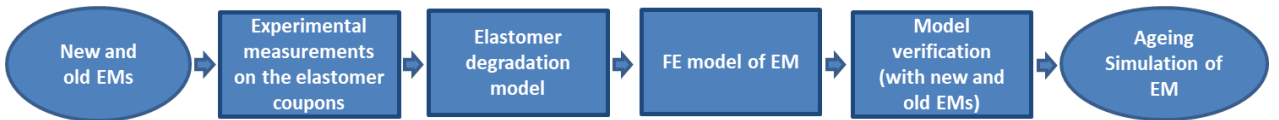Figure 3. Flowchart of the detailed procedure for creating the EM ageing model.

3. Elastomer Ageing Model

As described in Section 2, a realistic EAM should be able to simulate the change in material properties of the elastomeric MS under different ageing conditions. A set of EMs of the same vehicle model have therefore been provided. These ex-service EMs were removed from customers' vehicles in United Arab Emirates

(where EMs usually experience elevated temperature and high level of humidity), and reflected a range of different distance travelled. So they were all aged under real and relatively similar environmental conditions. The characteristics of these EMs used for creating the EAM are shown in Table 1.

Table 1. First batch of ex-service EMs used for creating the EAM

EM ID Number[†]	Distance Travelled (km)
U1_0 (New)	0
U1_1	37,517
U1_2	71,266
U1_3	120,356
U1_4	162,135
U1_5	163,804
U1_6	184,163

To capture the variation of mechanical properties of the material, coupons of the elastomer were taken from the MS of all the EMs listed in Table 1. These coupons were cut from the highlighted area in Figure 4-a which experiences maximum strain and mechanical deformation in the MS[‡]. This zone is also simultaneously in contact with the air from its exterior surface and the fluid from the interior surfaces (see Figure 1-b). Therefore, it is reasonable to assume that the elastomer located in this zone degrades significantly more than other areas in the MS.

[†] A selection of the UAE mounts representative of the full range of distance travelled.

[‡] This can be easily observed using the FE model of the EM, described in Section 4.

Figure 4 Coupons sample preparation of the elastomer from the highlighted zone, (a) longitudinal section of the MS (b) transverse sectioning of the MS.

DMTA is often carried out to measure mechanical properties of elastomeric materials [20]. The storage modulus and G' and the loss modulus G'' are the mechanical properties which are measured using DMTA. The magnitude of the equivalent shear modulus $G*$ can then be calculated from $|G^*| = G'\sqrt{1 + tan^2(\delta\,)}$ where $tan(\delta\,)$ is the mechanical loss factor defined as $tan(\delta\,)= G''/G'$ [21].

Analysis was conducted using a PerkinElmer 8000 in shear configuration with the rig mount shown in Figure 5. A dynamic temperature scan programme was utilised, measuring the storage shear modulus and $tan(\delta)$ of the samples. Measurements were taken over a temperature range from ambient temperature (28°C) up to 250°C with an incremental increase of temperature at a rate of $3°C/s$. This temperature range covers the upper range of operating conditions for the EMs in hot countries like UAE.

Coupons of the elastomer
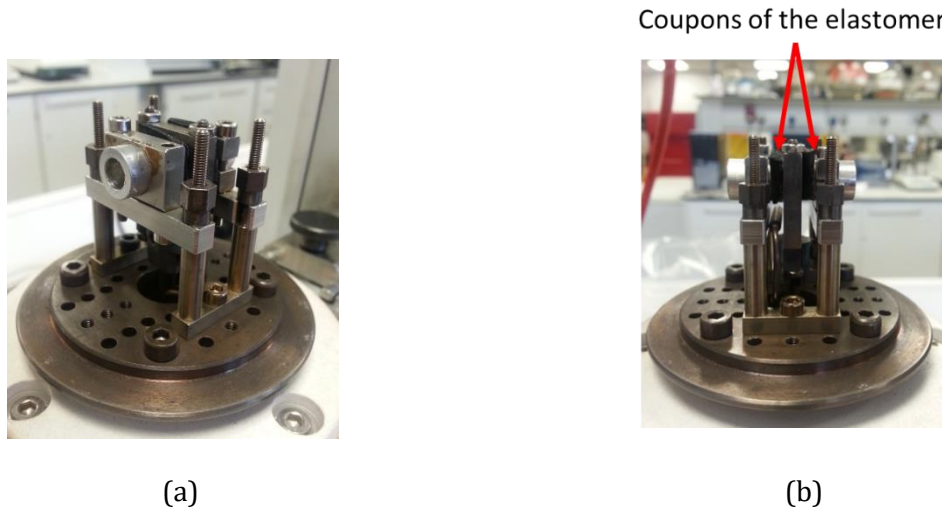
(a)   (b)

Figure 5 DMTA experimental set-up, (a) the isometric view (b) the front view.

Figure 6-a shows the variation of shear storage modulus G' with temperature for the EMs tested. Two trends can be observed in this figure:

- A decrease in storage modulus of ≤ 0.15 MPa up to about 50 °C followed by a gradual increase in G' of ≤ 0.15 MPa up to about 160°C followed by a steep decrease in G' up to 200°C (for New($U1\_0$), $U1\_1$, and $U1\_2$).

- An exponential decrease in G' up to approx. 160 °C followed by a steep decrease in storage modulus between 160 and 200°C (for $U1\_3$, $U1\_4$, $U1\_5$ and $U1\_6$).

The results for the damping property $tan(\delta)$ of the elastomeric coupons from the EMs listed in Table 1 also show a clear trend (Figure 6-b). The damping of the elastomers decreases with temperature while the reduction rate is more severe at low temperature (below 55 °C).
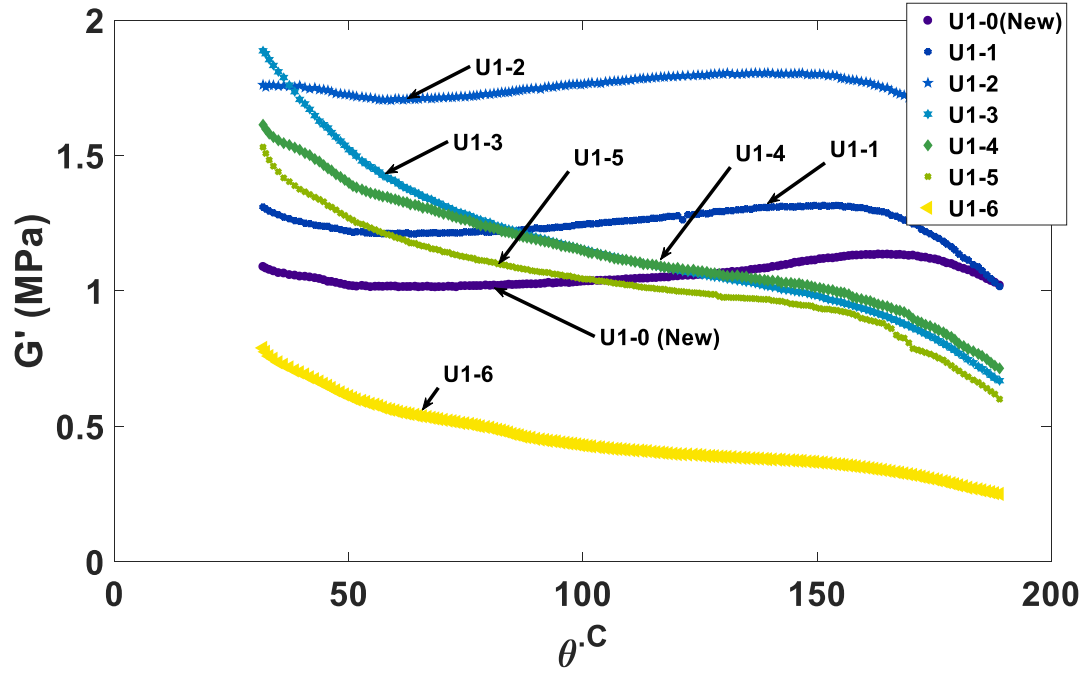
(a)
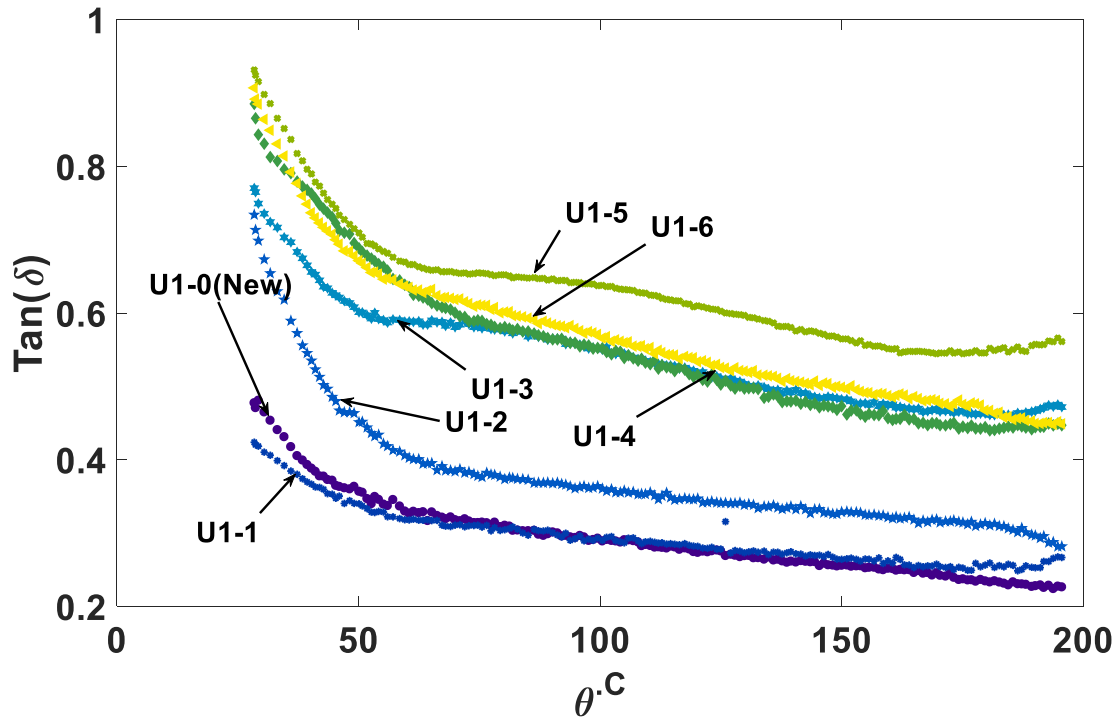
(b)

Figure 6. DMTA results :(a) Shear storage modulus *G'* and (b) *tan(δ)* against temperature for the elastomers of the different EMs.

The elastomer degradation model was created using this DMTA data. This material model contains information about the stiffness and damping changes against temperature and distance travelled. A MATLAB code was written based on

12

optimization and data regression techniques. This code numerically calculates the optimum value for the equivalent tensile elastic modulus, E_{eq} (i.e. $2|G^*|(1+\nu)$; where ν is Poisson's ratio), at each specific temperature θ and specific normalized distance travelled index $X \equiv distance\ travelled(km)/100{,}000km$ (or simply the age) from the elastomer degradation data. The current material ageing model is abridged in the following form:

$$E_{eq} = \sum_{i=0}^{m}\left(\sum_{j=0}^{n} a_{ij} X^j\right)\theta^i,$$ (1)

where *m=3* and *n=2* and the ageing coefficients a_{ij} are found in Table 2.

Table 2. Ageing coefficients a_{ij} used in Equation (1)

a_{ij}	j=0	j=1	j=2
i=0	*-0.9089*	*1.98178*	*1.2689*
i=1	*0.0093938*	*-0.024736*	*-0.0098395*
i=2	$-8.9705e-5$	*0.00019629*	*0.000118*
i=3	*2.9347e-7*	*-6.00612e-7*	*-3.7096e-7*

It should be noted that the material ageing model described by Equation (1) with coefficients given in Table 2, defines the equivalent Young's modulus of the elastomer in *MPa*. Elastic modulus values are then inserted into the FE model and the corresponding force-displacement curve and static stiffness K_{St} of the EM are calculated accordingly. The resultant stiffness ageing function of the EM describes the variation of K_{St} as a function of specific normalized distance travelled index X (or the age) and temperature θ.

4. FE Modelling of the Main Spring

As described in Section 2, the EM consists of different components and the only moving and flexible part is the MS. The MS enables the mount to transfer kinetic

energy from the engine to the internal fluid located in the compensation chamber and also contributes the static stiffness of the EM, K_{St}. The numerical model used in this study utilized the commercial FE package ABAQUS [22] to predict the variation of K_{St} due to the effect of material degradation of the elastomer during its lifespan. The assembled configuration of the main spring in ABAQUS is shown in Figure 7 with only half of the complete geometry considered in the model due to symmetry.
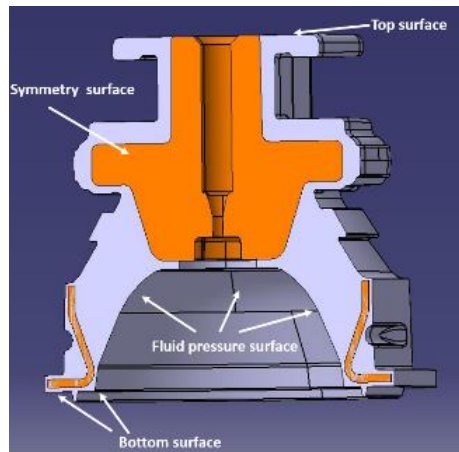

Figure 7 The symmetric geometrical ABAQUS model of the main spring (MS).

4.1. Meshing Details

The meshed model of the components along with the full meshed model of the MS are shown in Figure 8. The elastomeric part (Figure 8-a) is meshed using two types of elements. Three-dimensional tetrahedral ('tet') elements of type C3D10H are applied in the top area of the elastomer spring, where the elastomer does not deform severely, and 'hex' elements of type C3D20RH are used in the deformable areas of the rubber. This is done using a partitioning methodology which ensures that an appropriate number of 'hex' elements with uniform geometrical distribution are placed in the deformable areas of the MS. Both 'tet' and 'hex' elements also support hyper-elastic characteristics.

The aluminium rib which has an important effect on the stiffness of the MS is meshed using 'hex' elements of type C3D8R as seen in Figure 8-b. The aluminium
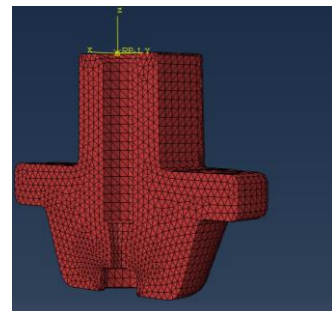
tip is meshed with 'tet' elements of type C3D4 (Figure 8-c). The tie constraint capability in ABAQUS is applied between the contact surfaces of the rubber and the rib and also between the elastomer and the tip, in order to bond the components together. The full meshed model of the MS is presented in Figure 8-d.
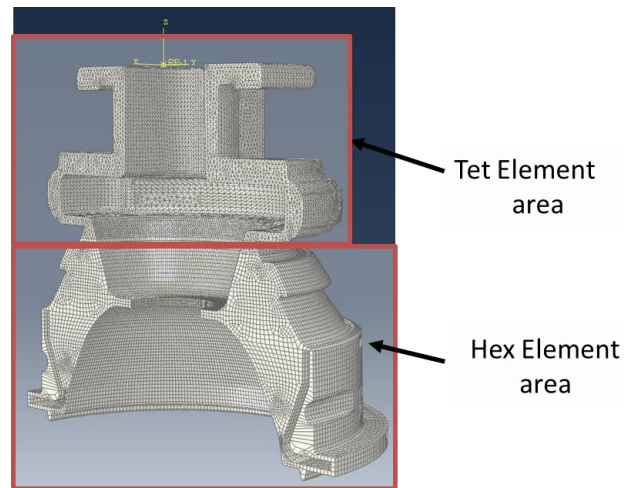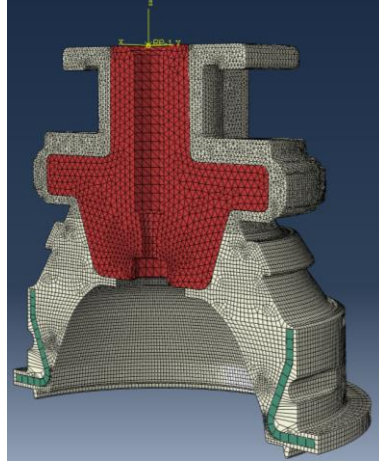

(a)
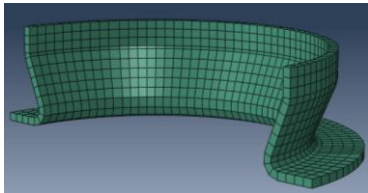
(b)

(c)

(d)

Figure 8 (a) The symmetric meshed model of the elastomeric spring, (b) the aluminium rib, and (c) the aluminium tip of the MS. (d) The full meshed model of the MS.

4.2. Boundary Conditions

Figure 7 depicts the external boundary conditions of the FE model of the MS. The bottom surfaces are stationary at the base of the EM, so the corresponding nodes are fixed in all degrees of freedom. The top surface is expected to experience a vertical displacement, *d,* in the *z*-direction, therefore nodes on that surface are constrained along *x* and *y* directions. To calculate the resultant reaction force on the top surface, a reference point (RP-1), tied to the top surface, is defined. The symmetry condition is also applied on the symmetry plane. The effect of the internal fluid on the MS is assumed as a uniform internal fluid pressure *P* acting on the internal surfaces which are in contact with the fluid. The internal fluid pressure is a function of relative dynamic displacements between the engine and chassis [8]. However, for static measurements, which is the subject of this paper, the effect of the fluid is assumed to be negligible (i.e. $P \cong 0$).

4.3. Material Properties

Elastomers are mostly considered as hyperplastic and incompressible materials. Several constitutive models such as Mooney–Rivlin, Ogden, Boyce-Arruda and Neo Hooke can be used to simulate their stress-strain behaviour

16

and to characterise their material properties [23]. However experimental stress-strain curves of the elastomer coupons cut from the MS of the new EM, with an example shown in Figure 9, clearly reveal that the stress-strain relation does not go beyond the linear regime (even for 15% strain) and the hyper-elastic behaviour of the elastomer is negligible within the strain range experienced by the MS during the operation of the EM. Moreover, a linear response is also observed from the compressive tensile test carried out on this type of EMs (Figure 10) up to a high vertical compressive displacement of 6mm. Thus, it is assumed that the elastomeric component of the new EM behaves elastically with an equivalent elastic modulus, *E,* measured as *E=3.7 MPa* from Figure 9 and a Poisson's ratio of $\nu \cong 0.499$ [24].
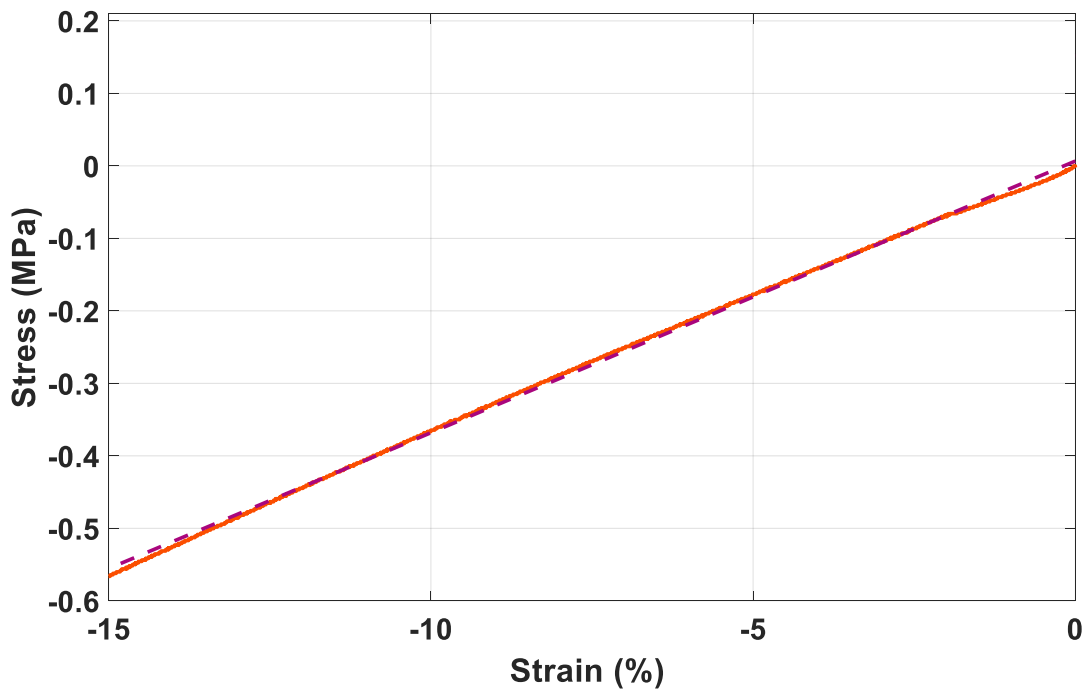

Figure 9 Experimental stress-strain curve of the coupons cut from new EM (solid line) with the linear data regression (dashed line).

The rib and the tip are made of a generic aluminium alloy with an elastic modulus of *70 GPa* and a Poisson's ratio of *0.3.*

4.4. FE Model Validation

To verify the accuracy of the FE model, a vertical compression of *d=6mm* is applied to the FE model and the total reaction force of the nodes located on the top surface of the tip is recorded as the static reaction force of the EM. Five new EMs were tested using a Tinius-Olsen 25kN machine under a similar condition, as shown in Figure 10-a. A 6 mm vertical compression displacement is applied to the EMs and the reaction forces of the tip are measured. The displacement rate is set to 1 mm/min to maintain static loading conditions and to avoid any dynamic effects of the internal fluid. The experimental force-displacement curves of these new EMs along with the FE result are plotted in Figure 10-b. The static stiffness of the EM is obtained by calculation of the slope of the curves. A summary of the measured stiffness values and the simulated stiffness are given in Table 3. The stiffness values and also the F-d curves validate the FE prediction in terms of the static behaviour of the EM with good agreement between experimental and modelling results.
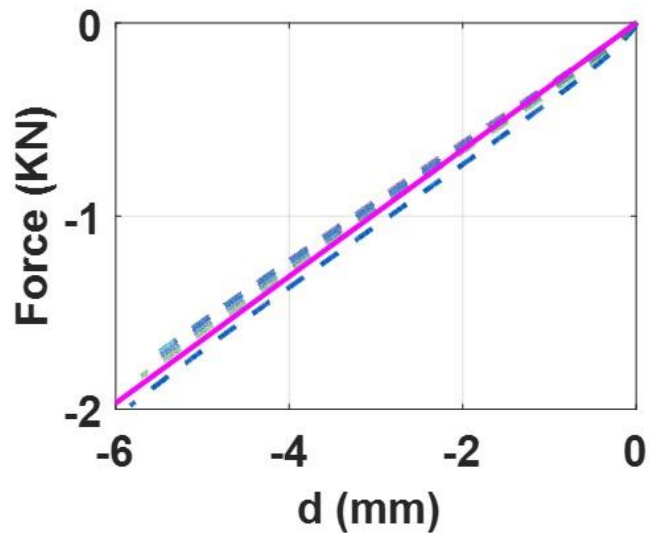
(a)   (b)

Figure 10 (a) Tensile testing setup for the new EMs and (b) a comparison between load-displacement curves for new EMs (dashed lines) and simulated behaviour from the FE model (solid line).

Table 3. A comparison between the measured stiffness of the new EMs and simulated stiffness using FE model of the MS.

	K_{St}(N/mm)	Deviation from average (%)
New EM No1	309	-1.6
New EM No2	310	-1.3
New EM No3	334	+6.3
New EM No4	305	-2.9
New EM No5	313	+0.4
FE model	329	+4.7

5. Results and Discussion

The variation of the stiffness K_{St} with the distance travelled index X at $\theta = 30°C$ is plotted in Figure 11. To investigate the accuracy of this simulated ageing trend, an additional set of ex-service EMs (the second batch of old EMs at different ages-listed in Table 4) was obtained and tested using the setup shown in Figure 10-a.

Table 4. Second batch of ex-service EMs used for verifying the ageing trend of the EM.

EM ID Number	Distance Travelled (km)	EM ID Number	Distance Travelled (km)
U2_1	27231	U2_7	82249
U2_2	52257	U2_8	87792
U2_3	54002	U2_9	92041
U2_4	59867	U2_10	96638
U2_5	77955	U2_11	129996
U2_6	81491	U2_12	145926

The force-displacement curves were recorded and their corresponding static stiffness K_{St} values were calculated. These values are shown in Figure 11 along with the simulated ageing model. It should be highlighted again that the ageing model, whose results are presented in this figure, was built based on the results of the FE model coupled to the DMTA measurements of modulus in the first set of ex-service EMs (presented in Table 1). The comparison between experimental and modelling results reveals that the in-service ageing behaviour of EMs is correctly simulated by the modelling methodology developed in this work in terms of trend, with first an increase in stiffness followed by a decrease. Experimental stiffness values from the second batch of aged EMs are also reasonably well predicted, however, there are some differences between the simulated ageing trend and measured stiffness of the second batch of the aged EMs.

The first possible source of this difference are deviations in the stiffness of the new EMs. As presented in Table 3, the stiffness of the new EMs can deviate up to 6% from its average value (i.e. 314.2 N/mm). This deviation can be explained due to the design tolerance of the EM stiffness, so might be a source of the discrepancies observed in Figure 11. The other source, which is more important, is the real ageing conditions that each EM (in both batches) have experienced during their operational life in the vehicle. Obviously, each of them have aged under relatively similar temperatures but with unknown variability, environmental and dynamic loading conditions which are really hard to monitor and also definitely affect their mechanical behaviours. The number of the EMs used for creating the EAM a is another source of the differences. It should indeed be noted that collecting EMs from the same car model, at specific mileages and from the same environmental conditions (from the UAE in this study) was a major practical issue in this work. However two batches of aged EMs were successfully provided. The ageing model of the EM was created using the first batch of supplied EMs listed in Table 1 and 2 while the ageing prediction was validated using the EMs listed in Table 4.

Results, however, demonstrate the effectiveness of the developed modelling methodology with predictions that are expected to improve as more data become available over time.

According to the simulated ageing behaviour, two interesting ageing trends are observed:

- A hardening effect with an increase of stiffness with distance X is seen at $X<0.95$. This might potentially be the result of a post-curing mechanism, which has the effect of increasing cross-linking [25]. The increase in cross-link density results in an increase of stiffness [26] because the cross-links are strong intermolecular bonds which restrict the movement of the elastomer chains.
- For $X>0.95$, the ageing trend is reversed and a softening behaviour is observed. This stiffness reduction could be the result of the mechanical loading applied to the material, the Mullin's effect, which causes softening due to repeated cyclic loading during the lifetime of the EM under continuous dynamic loading [27].

  It should be emphasized that such hardening and, then, softening trend of the EM stiffness against the travelled distance of the vehicle and under real practical ageing conditions (not under lab conditions) has not been reported in the literature to the authors' best knowledge. The physical reasons and underlying mechanisms behind this trend are currently unknown. All the aforementioned ageing mechanisms might have contributed to this trend, but this would need confirmation through further work.

  The simulated trend can be used directly in practical applications, ageing design and dynamic simulations of the EM. Using the simulated ageing trends, the static stiffness of the EM is predicted at each distance travelled

and temperature under real conditions without need for further experimental tests on micromechanics of the elastomer.
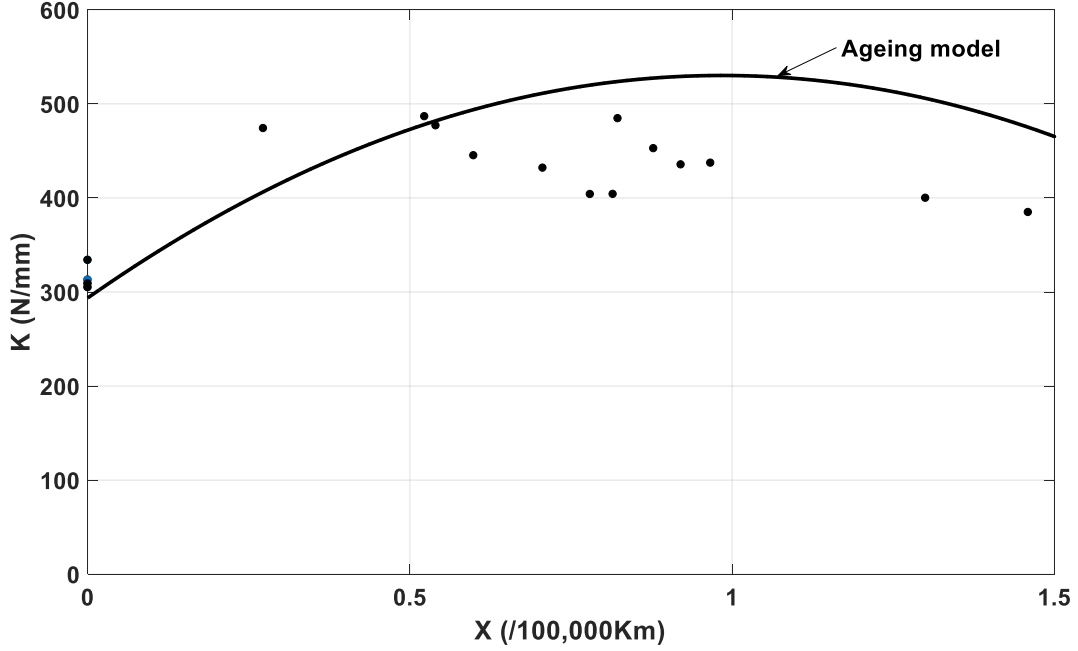

Figure 11 A comparison between the simulated ageing behaviour of EM against the normalized distance travelled index X (solid line) at $\theta = 30°C$ and the measured stiffness of the old EMs (the second batch) at different ages (scattered points)

The methodology described in Figure 3 also enables the stiffness ageing function to be calculated at different temperatures. Figure 12 represents the ageing behaviour of the EM at $\theta = 30, 50, 70,$ and $90°C$. The figure reveals that the stiffness peak of the ageing function occurs at lower travelled distance X as temperature θ increases together with a reduction in the level of maximum stiffness. It also clearly reveals that the model is sensitive to temperature change. An almost 20% reduction in both the stiffness and the age is observed when temperature increases to 90°C from normal ambient temperature.

Using this methodology, it is also possible to show the stiffness evolution of the EM against temperature θ for different X. Figure 13 shows that at low age, when the EM is still new, the stiffness change with temperature is almost negligible (see curves for X=0, 0.3). However, as X increases, stiffness clearly decreases with

22

temperature (curves for X=1, 1.3). It is also worth noting that the reduction of stiffness with temperature becomes more significant beyond 100,000 km.
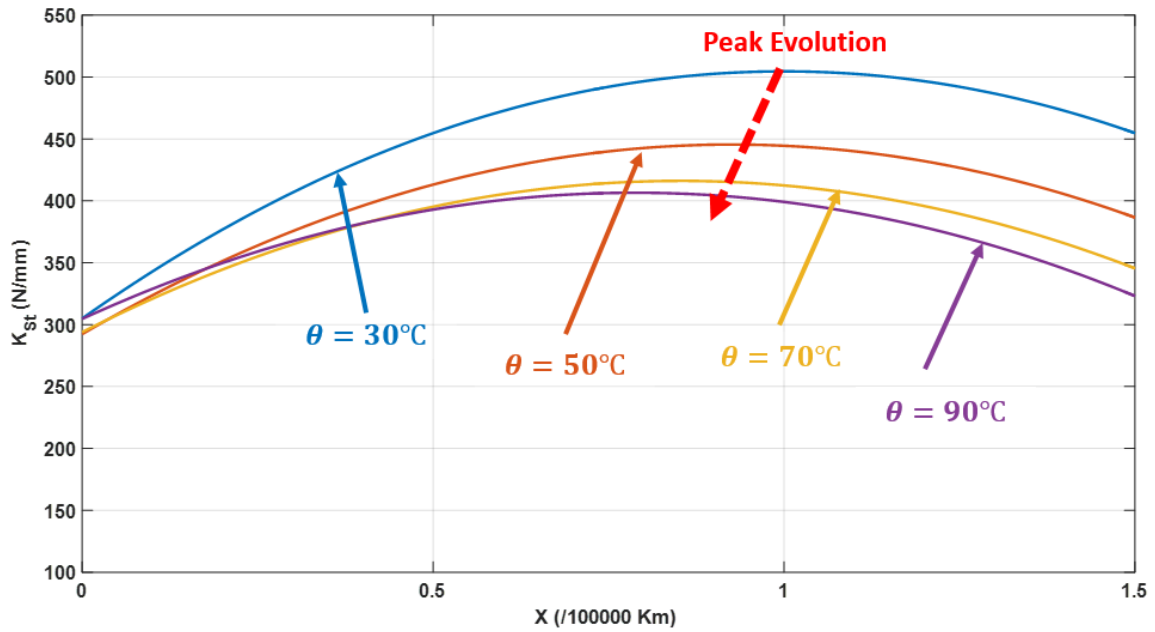

Figure 12 Variation of the axial EM stiffness K_{st} against the normalized distance travelled index X. at different temperatures θ.
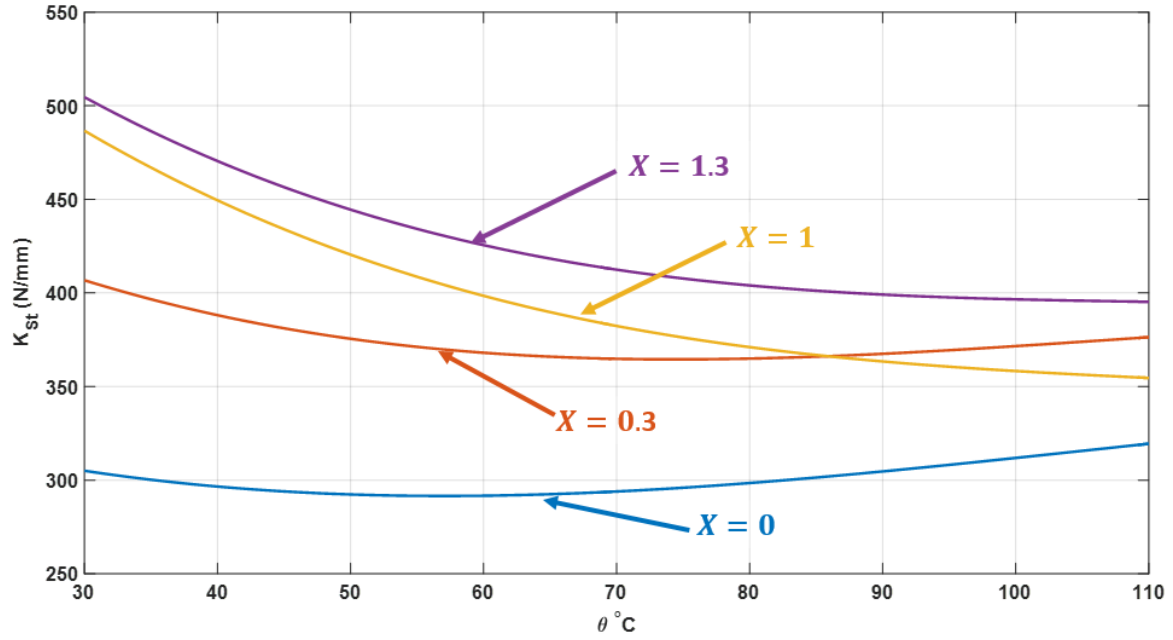
Figure 13 Variation of the axial EM stiffness K_{st} against temperature θ at different normalized distance travelled indexes X.

6. Conclusion

This paper describes a practical methodology for the simulation of the ageing behaviour of EMs used in-service. Ageing occurs in EMs due to changes in stiffness and material properties of its elastomeric MS during the operational lifetime of the vehicle. The material ageing model of the elastomer was built up using experimental DMTA tests on the elastomer coupons cut from a set of ex-service EMs. The FE model of the MS run with the obtained ageing material characteristics and the ageing function was created. This function characterises the variation of the static stiffness against vehicle distance travelled (or age). Results show a hardening behaviour up to a certain distance (about *95000* km) with stiffness values increasing by up to 57% followed by a softening phase for higher distances with stiffness values tending towards original values. It was also shown that the maximum stiffness occurs at lower distances with lower stiffness values as the temperature increases. A reduction of 20% is observed on the stiffness peak as the temperature increases to 9*0*°C from *30*°C.

The main contributions of this research can be summarised as follows:

1. A new modelling methodology has been developed to simulate the variation of EMs stiffness with mileage and temperature due to real conditions (as opposed to lab conditions) ageing of their constitutive elastomer. This practical data-based approach makes use of a limited number of experiments and has proven effective in predicting the mechanical response of EMs not used to train the model, with an accuracy expected to improve as more data become available.

2. Modelling results reproduce the hardening and, then, softening trend of the EM stiffness with mileage, which has not been previously reported. The underlying ageing mechanisms of the elastomer responsible for this trend are currently unknown and further work is therefore needed to provide a physical explanation.

3. The outcome from this work provides the automotive industry with new opportunities to understand the influence of ageing on the mechanical response of elastomer-based components and to account for it at the design stage.

7. Acknowledgment

List of Abbreviations and Acronyms:

	Definition
DMTA	Dynamic mechanical thermal analysis
EAM	Elastomer Ageing Model
EM	Engine Mount

FE	Finite Element
MS	Main Spring
NVH	Noise, Vibration and Harshness
UAE	United Arab Emirates

References:

1. Le Saux, V., et al., *Limits in the validity of Arrhenius predictions for field ageing of a silica filled polychloroprene in a marine environment.* Polymer Degradation and Stability, 2014. **99**: p. 254-261.

2. Somers, A., et al., *Quantifying rubber degradation using NMR.* Polymer degradation and stability, 2000. **70**(1): p. 31-37.

3. Jha, A. and A. Bhowmick, *Thermal degradation and ageing behaviour of novel thermoplastic elastomeric nylon-6/acrylate rubber reactive blends.* Polymer degradation and stability, 1998. **62**(3): p. 575-586.

4. Bhowmick, A. and J. White, *Thermal, UV-and sunlight ageing of thermoplastic elastomeric natural rubber-polyethylene blends.* Journal of materials science, 2002. **37**(23): p. 5141-5151.

5. Lewitzke, C. and P. Lee, *Application of elastomeric components for noise and vibration isolation in the automotive industry.* 2001, SAE Technical Paper.

6. Sung, D.-U., J. Busfield, and Y.H. Ryu, *Degradation of Vehicle Noise and Vibration by Ageing of Elastomers.* 2017, SAE Technical Paper.

7. Ngolemasango, F.E., M. Bennett, and J. Clarke, *Degradation and life prediction of a natural rubber engine mount compound.* Journal of applied polymer science, 2008. **110**(1): p. 348-355.

8. Christopherson, J. and G.N. Jazar, *Dynamic behavior comparison of passive hydraulic engine mounts. Part 1: Mathematical analysis.* Journal of Sound and Vibration, 2006. **290**(3): p. 1040-1070.

9. Ngolemasango, E., M. Bennett, and J. Clarke, *Kinetics of the effect of ageing on tensile properties of a natural rubber compound.* Journal of applied polymer science, 2006. **102**(4): p. 3732-3740.

10. Woo, C.S. and W.D. Kim, *Heat-aging effects on the material properties and fatigue life prediction of vulcanized natural rubber.* e-Journal of Soft Materials, 2006. **2**: p. 7-12.

11. Woo, C.S., et al., *Useful lifetime prediction of rubber components using accelerated testing.* IEEE Transactions on Reliability, 2010. **59**(1): p. 11-17.

12. Colgate, J., et al., *Modelling of a hydraulic engine mount focusing on response to sinusoidal and composite excitations.* Journal of Sound and Vibration, 1995. **184**(3): p. 503-528.

13. Gent, A.N., *Engineering with rubber: how to design rubber components.* 2012: Carl Hanser Verlag GmbH Co KG.

14. Rattanasom, N., T. Saowapark, and C. Deeprasertkul, *Reinforcement of natural rubber with silica/carbon black hybrid filler.* Polymer Testing, 2007. **26**(3): p. 369-377.

15. Choi, S.S., *Influence of rubber composition on change of crosslink density of rubber vulcanizates with EV cure system by thermal aging.* Journal of applied polymer science, 2000. **75**(11): p. 1378-1384.

16. Gwaily, S., et al., *Influence of thermal aging on crosslinking density of boron carbide/natural rubber composites.* Polymer testing, 2003. **22**(1): p. 3-7.

17. Cunneen, J., *Oxidative aging of natural rubber.* Rubber chemistry and technology, 1968. **41**(1): p. 182-208.

18. Ignatz-Hoover, F., et al., *Chemical additives migration in rubber.* Rubber chemistry and technology, 2003. **76**(3): p. 747-768.

19. Lewis, J.E., M.L. Deviney Jr, and L.E. Whittington, *Migration of Antioxidants and Accelerators in Natural and Synthetic Rubber II. Sulfenamide System Studies and Comparison of Age Resister Migration under Inert and Practical Conditions.* Rubber Chemistry and Technology, 1969. **42**(3): p. 892-902.

20. Ahmad, Z., M. Sarwar, and J. Mark, *Dynamic-mechanical thermal analysis of aramid-silica hybrid composites prepared in a sol-gel process.* Journal of applied polymer science, 1997. **63**(10): p. 1345-1352.

21. Menard, K.P., *Dynamic mechanical analysis: a practical introduction*. 2008: CRC press.

22. ABAQUS, V., *6.14 Documentation.* Dassault Systemes Simulia Corporation, 2014.

23. Kim, B., et al., *A comparison among Neo-Hookean model, Mooney-Rivlin model, and Ogden model for chloroprene rubber.* International Journal of Precision Engineering and Manufacturing, 2012. **13**(5): p. 759-764.

24. Coveney, V.A., *Elastomers and Components: Service Life Prediction-Progress and Challenges*. 2006: Woodhead Publishing.

25. Mathew, A.P., S. Packirisamy, and S. Thomas, *Studies on the thermal stability of natural rubber/polystyrene interpenetrating polymer networks: thermogravimetric analysis.* Polymer Degradation and Stability, 2001. **72**(3): p. 423-439.

26. Zimmer, G., A. Guthausen, and B. Blümich, *Characterization of cross-link density in technical elastomers by the NMR-MOUSE.* Solid state nuclear magnetic resonance, 1998. **12**(2): p. 183-190.

27. Cantournet, S., R. Desmorat, and J. Besson, *Mullins effect and cyclic stress softening of filled elastomers by internal sliding and friction thermodynamics model.* International Journal of Solids and Structures, 2009. **46**(11): p. 2255-2264.